Ultrasound irradiation synthesis of novel copper(II) complex with the 2-thiophenimidazoline ligand: SC-XRD, HSA, and DFT study

Hadi Kargar, Mehdi Fallah-Mehrjardi, Necmi Dege, Muhammad Ashfaq, Khurram Shahzad Munawar, Muhammad Nawaz Tahir, Mehdi Sahihi, Mahdieh Asgari Bajgirani

Ultrasound irradiation synthesis of novel copper(II) complex with the 2-thiophenimidazoline ligand: SC-XRD, HSA and DFT study

Hadi Kargar [a,*], Mehdi Fallah-Mehrjardi [b], Necmi Dege [c], Muhammad Ashfaq [d], Khurram Shahzad Munawar [e,f], Muhammad Nawaz Tahir [d], Mehdi Sahihi [g], Mahdieh Asgari Bajgirani [h]

[a] Department of Chemical Engineering, Faculty of Engineering, Ardakan University, P.O. Box 184, Ardakan, Iran.

[b] Department of Chemistry, Payame Noor University (PNU), 19395-4697, Tehran, Iran

[c] Department of Physics, Faculty of Arts and Sciences, Ondokuz Mayıs University, 55139, Samsun, Turkey

[d] Department of Physics, University of Sargodha, Sargodha 40100, Pakistan

[e] Institute of Chemistry, University of Sargodha, Sargodha, 40100, Pakistan

[f] Department of Chemistry, University of Mianwali, Mianwali, 42200, Pakistan

[g] Université Clermont Auvergne, CNRS, Clermont Auvergne INP, Institut de Chimie de Clermont-Ferrand, F-63000 Clermont-Ferrand, France

[h] Department of Physical Chemistry, Faculty of Chemistry, Lorestan University, Lorestan, Iran

Abstract

A novel coordination **$CuCl_2(L)_2$** complex was synthesized by complexation of the 2-thiophenimidazoline ligand with $CuCl_2.2H_2O$ in less than 10 minutes. The synthesis was done using ultrasound irradiation in an ethanol solvent. The complexation was confirmed using CHN and FT-IR analysis and linked to the theoretical IR and DFT calculations. The single crystal X-ray diffraction approach was employed to figure out the arrangement of atoms in the crystal structure of the **$CuCl_2(L)_2$** complex. The copper ion is coordinated by two symmetry related non-chelating 2-

* Corresponding author's e-mail: h.kargar@ardakan.ac.ir

thiophenimidazoline ligands and two symmetry related chlorine atoms. 2-thiophenimidazoline ligands coordinate with the metal center by N-atom, whereas S-atom does not coordinate with the metal center. The X-ray results revealed a square planar coordination geometry, as evident from the respective bond angles around the Cu(II) ion. Hirshfeld surface analysis was done to learn more about intermolecular contacts. Theoretical calculations were carried out using DFT employing the B3LYP/Def2-TZVP level of theory, which showed that theoretical conclusions were reliable with experimental data.

Keywords: Copper(II), 2-Thiophenimidazoline, SC-XRD, HSA, Theoretical studies

Introduction

Imidazoline is a five-membered heterocyclic ring holding two nitrogens and is formed by reducing one of the two double bonds in imidazoles [1]. Imidazoline is a common chemical found in many natural and pharmaceutical medicines. Additionally, these scaffolds are utilised as an intermediary in the production of many organic scaffolds [2]. Furthermore, chiral imidazolines are commonly used as organocatalysts in the production of widespread natural and synthetic organic molecules [3]. There has been a rise in interest in discovering novel ways to synthesize these imidazoline analogues during the last decade. Major advancement is made in both the modification of already known procedures and the introduction of new approaches [1,4]. Aside from their luminous features, imidazoline derivatives exhibit a variety of pharmacological potentials and engage in a variety of important metabolic processes [5–7].

Imidazolines are entirely sigma-donors in nature. To the best of our knowledge, there is no indication of back donation through π-bonding in metal-imidazoline complexes, which can be explained by the existence of the π-donor pyrrole-like NH centre [8]. For many years, researchers have been interested in the study of imidazolines as a complexing agent, primarily because it is engaged in many biological processes [9]. The deprotonated nitrogen atom can connect to the metal ions, and several complexes that involve imidazoline and other metal ions have been described [10,11]. The protonated nitrogen

atom of the imidazoline ring, however, is an excellent hydrogen bond donor, and hence, it is involved in the interactions concerning the hydrogen bonds that can result in the formation of multi-dimensional supramolecular structures [12].

Copper is a necessary trace metal that plays a vital function in numerous physiological and biological processes [13]. It contributes to the production of haemoglobin and the proper functioning of the thyroid gland due to its properties as an endogenous element to act as an antioxidant and a pro-oxidant. [14]. Furthermore, its activity as a cofactor in various enzyme processes has been extensively researched [15].

Copper complexes in which copper has +1 and +2 oxidation states exhibit promising anticancer properties, which has resulted in the research of copper complexes that comprise therapeutic families of ligands such as imidazolines, thiosemicarbazones, and phosphines [16]. Imidazoline-based copper complexes have been employed as potent anti-cancer drugs as well as for other therapeutic purposes [17,18].

The occurrence of copper imidazoline complexes in proteins including amine oxidases, azurin, oxygen-binding hemocyanins, and others has continuously encouraged scientists to explore their structural chemistry [19–21].

We recently published a copper(I) complex employing the same ligand and explored its structural features both experimentally and theoretically [22]. Hence, in continuation of our research on copper complexes [23–28], the present investigation emphasises on synthesis and structural exploration of copper complex with an imidazoline-based ligand to discover the molecular and supramolecular structural assemblies.

Results and discussion

Synthesis

The **$CuCl_2(L)_2$** complex was produced by reacting 2-thiophenimidazoline with copper(II) chloride dihydrate in ethanol under ultrasonic irradiation for 10 min (Scheme 1).

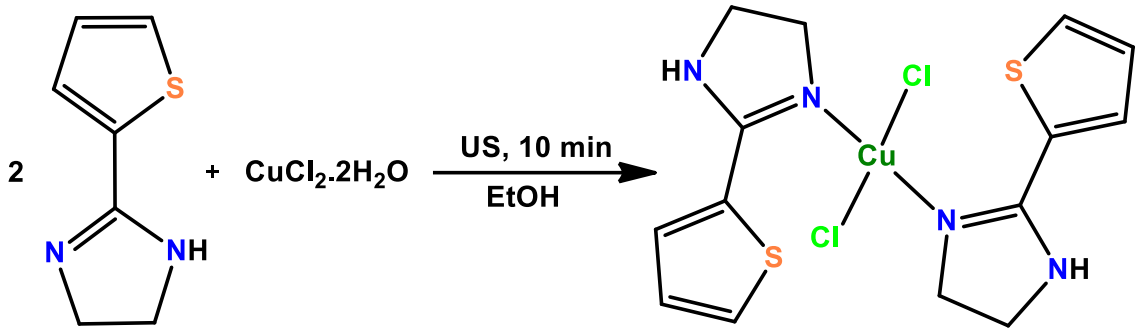

Scheme 1. Synthesis of **$CuCl_2(L)_2$** complex under ultrasound irradiation.

Crystal structure analysis

The asymmetric unit of **$CuCl_2(L)_2$** contained half a molecule, and the molecule is completed by inversion symmetry at point (2,1,1) (Fig. 1, Table 1). The copper is bonded to two symmetry-related non-chelating 2-thiophenimidazoline ligands and two symmetry related chlorine atoms. These ligands coordinate with the metal center by the N–atom, whereas the S-atom does not coordinate with the metal center. Cu–N bond length is shorter than Cu–Cl bond length (Table 2), and bond angles in the coordination sphere have a span from 89.80 (8) to 180.0°, showing that coordination geometry is square planar. Torsion angles Cl1–Cu1–N1–C1 and Cl1–Cu1–N1–C3 are -84.7 (3) and 96.1 (4)°, respectively. 2-thiophenimidazoline is almost planar, as the dihedral angle between 4,5-dihydro-1H-imidazole ring A (C1–C3/N1/N2) and thiophene ring B (C4–C7/S1) is 3.4 (3)°. The crystal structure of 2-thiophenimidazoline is reported in the literature with reference code ROMDIH [29]. The dihedral angle among the rings in ROMDIH is 5.17 (10)°, which is larger than the dihedral angle between the same rings in **$CuCl_2(L)_2$**. A closely related copper complex of the same ligand and iodine atom is reported in the literature with reference to a code WAPFOM [22]. In WAPFOM, the 2-thiophenimidazoline ligand behaves as a chelating ligand. Two 2-thiophenimidazoline ligands chelate copper metal in WAPFOM, with dihedral angles between rings, are 12.02 (1)° and 2.4 (2)° in the first and second ligands, respectively. The molecular units are interconnected *via* N–H···Cl in the shape of dimers and generate a $R_2^2(12)$ loop [30]. Infinite C(6) chains are created by N–H···Cl bonding that prolongs beside the *a*-axis (Fig. 2, Table 3). The orientation of the molecule is such that chloride ions

of one molecule form H-bonding interactions with NH groups of the neighbouring molecules and the NH groups are opposite to the S-atoms of the symmetry related molecule. The presence of two chloride ions in the coordination sphere prevents S-atoms to coordinate with the metal center. S-atoms play an important role in the stabilization of molecular geometry as there are Cu···S, two N···S, three C···S and three H···S contacts within a molecule. S-atoms from a Cl···S, five C···S and seven H···S intermolecular contacts with a distance less than 4 Å. The crystal packing, or supramolecular assemblage, is stabilized by the off-set π···π interactions between similar and dissimilar rings having inter-centroid distances extending from 3.68 to 3.98 Å and slippage from 1.488 to 1.892 Å (Fig. 3).

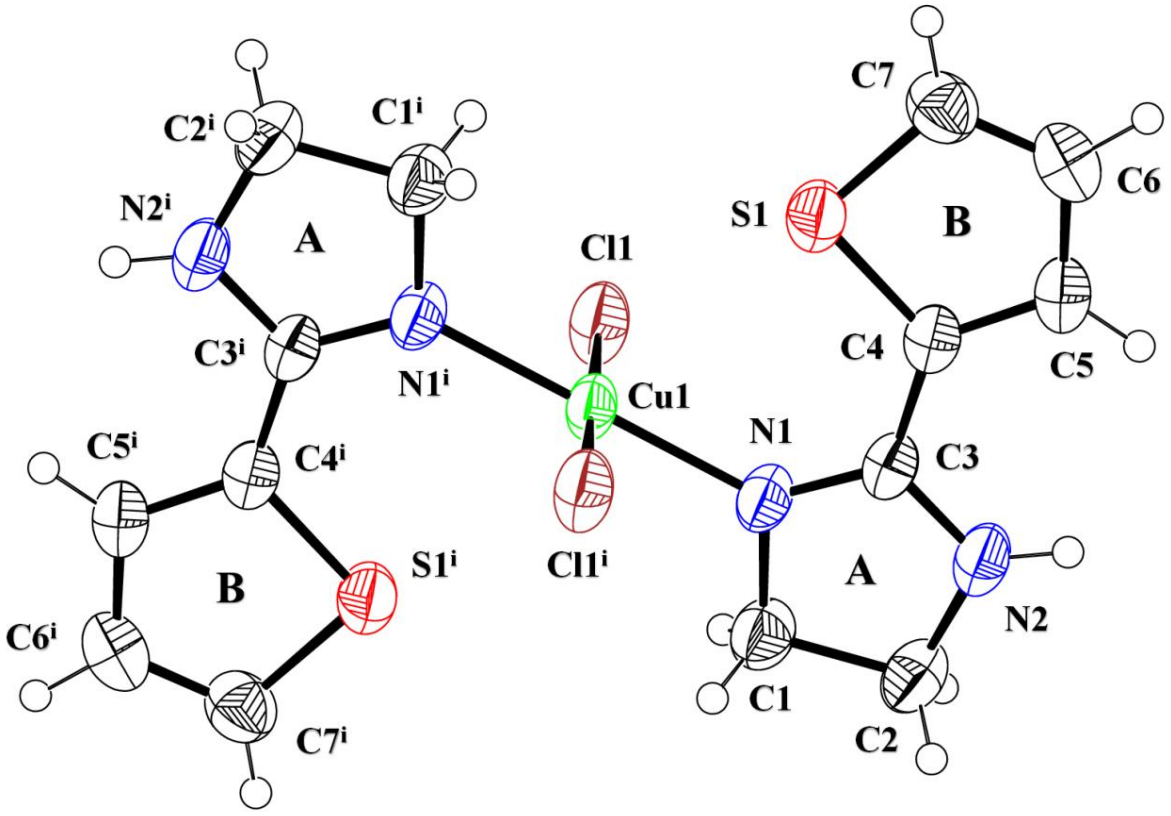

Fig. 1. ORTEP interpretation of **$CuCl_2(L)_2$** at a 50% likelihood level. The H-atoms are characterized by means of tiny circles with adjustable radii.

Table 1. Crystal statistics and structural enhancement factors for **$CuCl_2(L)_2$** complex.

Chemical formula	**$C_{14}H_{16}Cl_2CuN_4S_2$**
Formula weight	438.87
Temperature (K)	293
Wavelength (Å)	0.71073
Crystal system	Triclinic
Space group	$P\bar{1}$

a (Å)	7.9773(10)
b (Å)	8.0947(11)
c (Å)	8.6530(11)
α (°)	115.726(12)
β (°)	99.291(13)
γ (°)	109.932(10)
Volume (Å^3)	440.52(11)
Z	1
Radiation type	Mo-*Kα*
μ (mm^{-1})	1.78
Crystal size (mm)	0.38 × 0.23 × 0.12
No. of measured, independent and observed [*I* >2s(*I*)] reflections	9610, 3845, 2116
R_{int}	0.099
$(\sin \theta/\lambda)_{max}$ (Å^{-1})	0.810
$R[F^2> 2\sigma(F^2)]$, $wR(F^2)$, *S*	0.057, 0.176, 1.05
No. of reflections	3845
No. of parameters	106
H-atom treatment	H-atom parameters constrained
$\Delta\rho_{max}$, $\Delta\rho_{min}$ (e Å^{-3})	0.69, −1.53

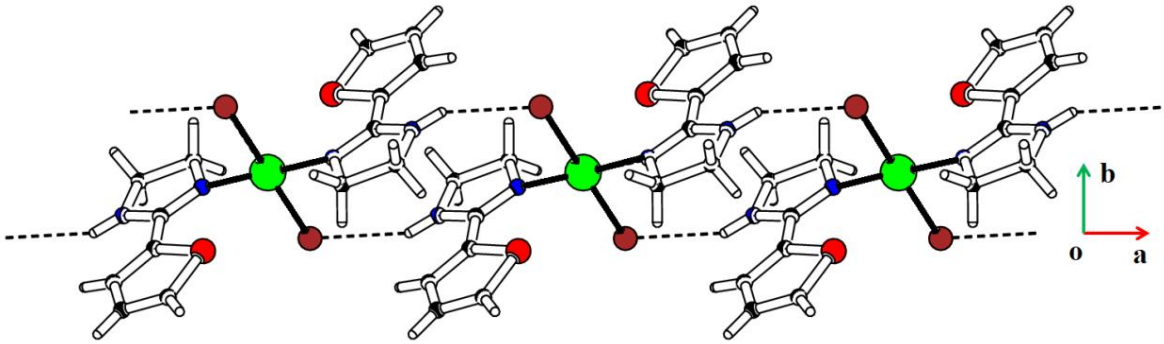

Fig. 2. Packing layout of **$CuCl_2(L)_2$** showing C(6) chain generated by N–H···Cl bonding.

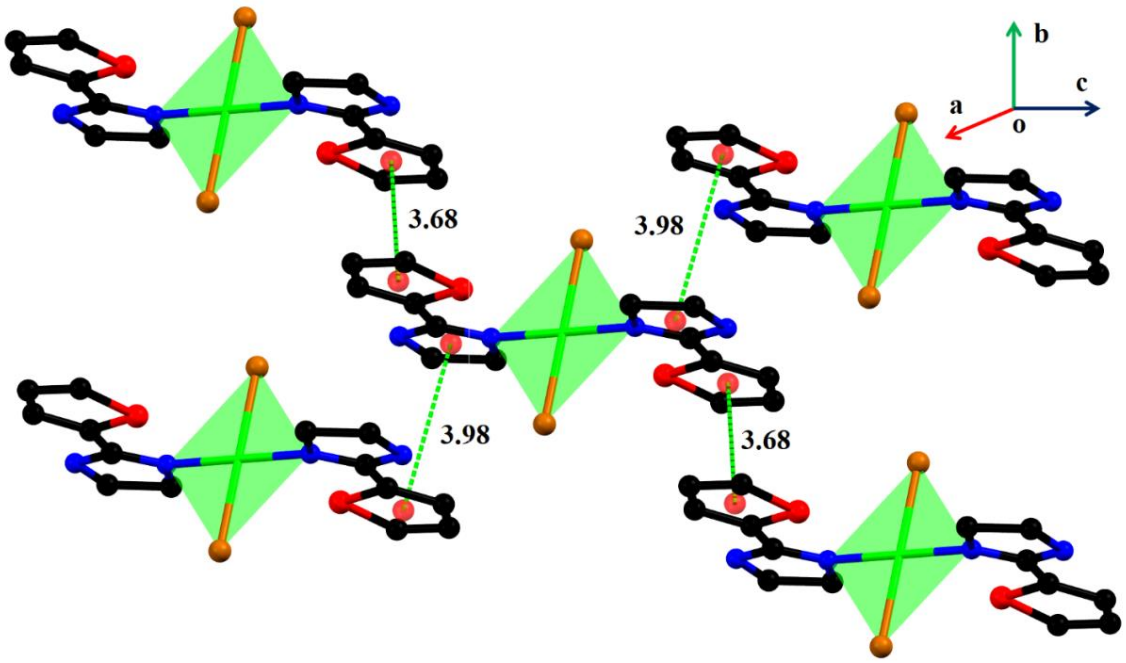

Fig. 3. A visual layout of off-set π···π interactions that connect molecules in *bc*-plane.

Table 2. Important bond distances (Å) and bond angles (°) of **$CuCl_2(L)_2$**. Symmetry code: (i) −x+2, −y+1, −z+1.

Bond distances		**Bond angles**	
Cu1—N1^{i}	1.952 (2)	N1^{i}—Cu1—N1	180.0
Cu1—N1	1.952 (2)	N1^{i}—Cu1—Cl1^{i}	89.80 (8)
Cu1—Cl1^{i}	2.3307 (10)	N1—Cu1—Cl1^{i}	90.20 (8)
Cu1—Cl1	2.3306 (10)	N1^{i}—Cu1—Cl1	90.20 (8)
N1—C3	1.307 (4)	N1—Cu1—Cl1	89.80 (8)
N1—C1	1.482 (4)	Cl1^{i}—Cu1—Cl1	180.0

Table 3. Hydrogen-bond geometry (Å, º).

D*—H···*A	***D*—H**	**H···*A***	***D*···*A***	**<*(D*—H···*A)*°**
N2—H2···Cl1^{ii}	0.86	2.54	3.326 (3)	152

Symmetry codes: (ii) *x*−1, *y*, *z*.

Hirshfeld surface analysis (HSA)

The intermolecular interactions are investigated in **$CuCl_2(L)_2$** in terms of short and long contacts by performing HSA, which is managed by means of Crystal Explorer version 21.5 [31]. Fig. 4a is the HS plotted over normalized distances (d_{norm}) for **$CuCl_2(L)_2$**. The surface uses red and blue regions to show short and long connections, correspondingly. The white stripes symbolise the contacts that are separated by the sum of Van der Waal's radii [32−34]. The red spots around chlorine, NH group and particular CH show that these atoms form short contacts. The regions in dashed black circles on the surface plotted over the shape index revealed stacking interfaces in **$CuCl_2(L)_2$** (Fig. 4b).

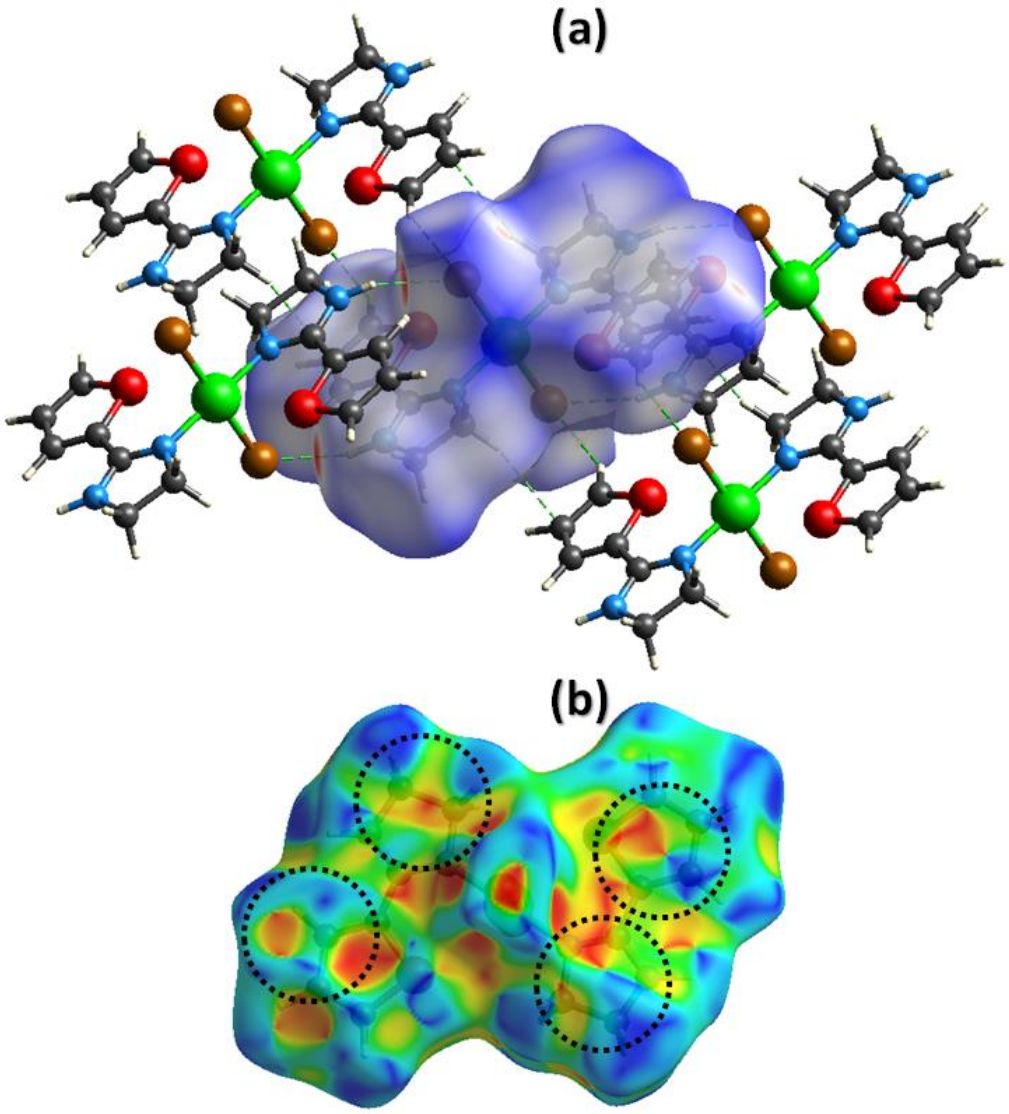

Fig. 4. HS plotted over (a) d_{norm} varies from -0.3082 to 1.3771 a.u, (b) shape index varies from -1 to 1 a.u.

2D plot analysis delivers statistics regarding the involvement of individual contacts in crystal packing [35–37]. Fig. 5a depicts a 2D plot for overall interactions with a pair of large spikes representing H···Cl contacts. The most significant contact is H···H with a 41.5% contribution to the overall interactions (Fig. 5b). The further important contacts are H···Cl, H···C, H···S, and C···C having 26.3%, 13.3%, 9.6%, and 4.8%, contributions, respectively. The enrichment ratio gives a propensity of pair of moieties responsible for crystal packing interactions [38,39]. The pairs that are favourable to form short contacts have an enrichment ratio greater than one. The pairs and their enrichment ratio are listed in Table 4. Moreover, voids are calculated by using the idea of pro-crystal electron density

and the result of the void analysis is mentioned in the supplementary information file (Fig. S1).

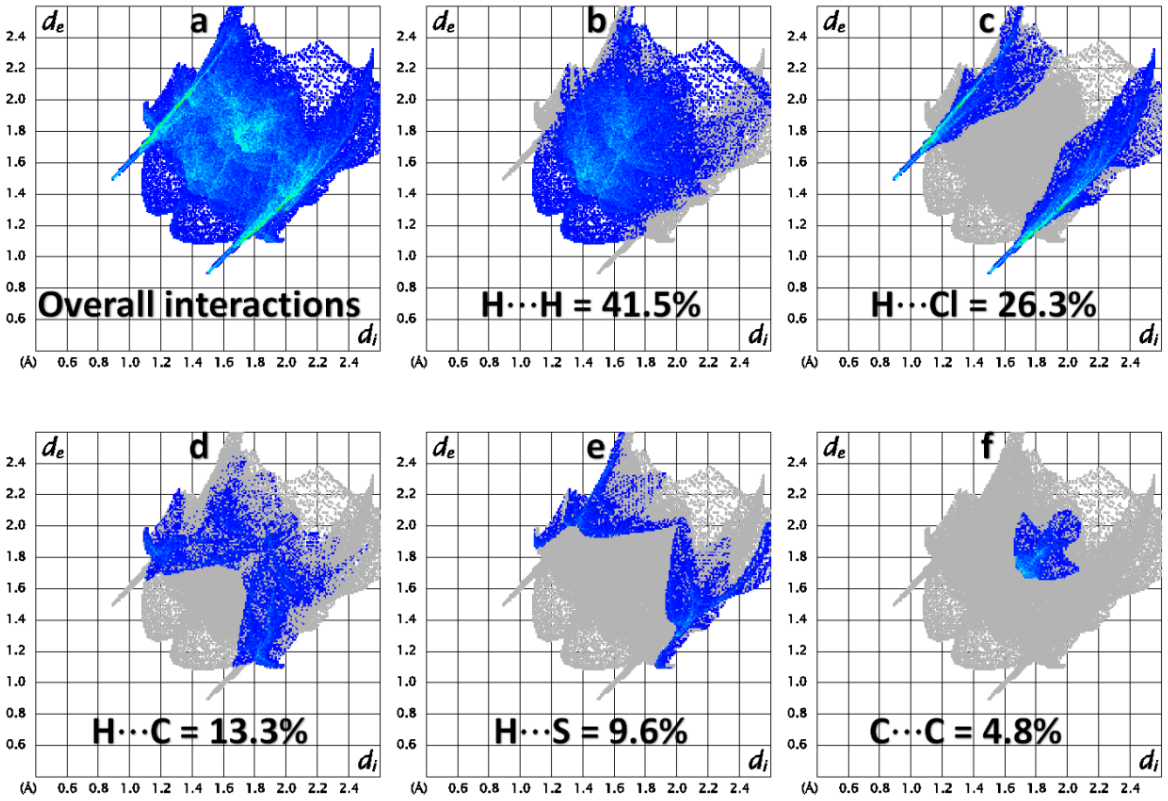

Fig. 5. 2D plot for (a) overall and (b-f) important interatomic interactions.

Table 4. Enrichment ratio for the pair of moieties present in **$CuCl_2(L)_2$**. It is not listed for the pairs having arbitrary contacts with less than 0.9% contribution.

	Atom	**H**	**C**	**N**	**S**	**Cl**	**Cu**
	H	41.5	13.3	2	9.6	26.3	
	C	13.3	4.8	2	0.5		
Contact %	**N**	2	2				
	S	9.6	0.5				
	Cl	26.3					
	Cu						
Surface%		67.1	12.7	2	5.05	13.15	0
	Atom	**H**	**C**	**N**	**S**	**Cl**	**Cu**
	H	45.02					
	C	17.04	1.61				
Random Contacts %	**N**	2.68	0.51	0.04			
	S	6.78	1.28	0.20	0.26		
	Cl	17.65	3.34	0.53	1.33	1.73	
	Cu	0.00	0.00	0.00	0.00	0.00	0.00
	Atom	**H**	**C**	**N**	**S**	**Cl**	**Cu**
	H	0.92					
	C	0.78	2.98				
Enrichment ratio	**N**	0.75					
	S	1.42	0.39				
	Cl	1.49			0.00	0.00	
	Cu						

The interactions between the molecules might be explored with respect to interaction energy. The interaction energy is the summation of coulomb electrostatic, polarization, dispersion, and repulsion energies [40–42]. The second and third ones are always attractive, however, the last one is always repulsive. The coulomb electrostatic energy of a pair can be attractive or repulsive. A cluster of 3.8 Å is produced near the molecule present in the asymmetric unit, and interaction energy calculations are carried out on Crystal Explorer version 21.5 at the HF/3-21G electronic density approach. The calculations showed that coulomb and dispersion energies are dominant over the other kinds of energies. The. Fig. 6 shows energy frameworks for coulomb and dispersion energy in which molecule's centers are joined by cylinders whose width is proportionate to the intensity of the associated energy. Although for some pairs, the coulomb energy is higher as compared to dispersion energy, overall, dispersion energy is the most prominent. The total interaction energy is the largest for the pair having the smallest intermolecular distance (i.e., 7.98 Å) (Fig. 6c). The study inferred that the most significant role is played by dispersion energy for stabilization of supramolecular associations of **$CuCl_2(L)_2$**.

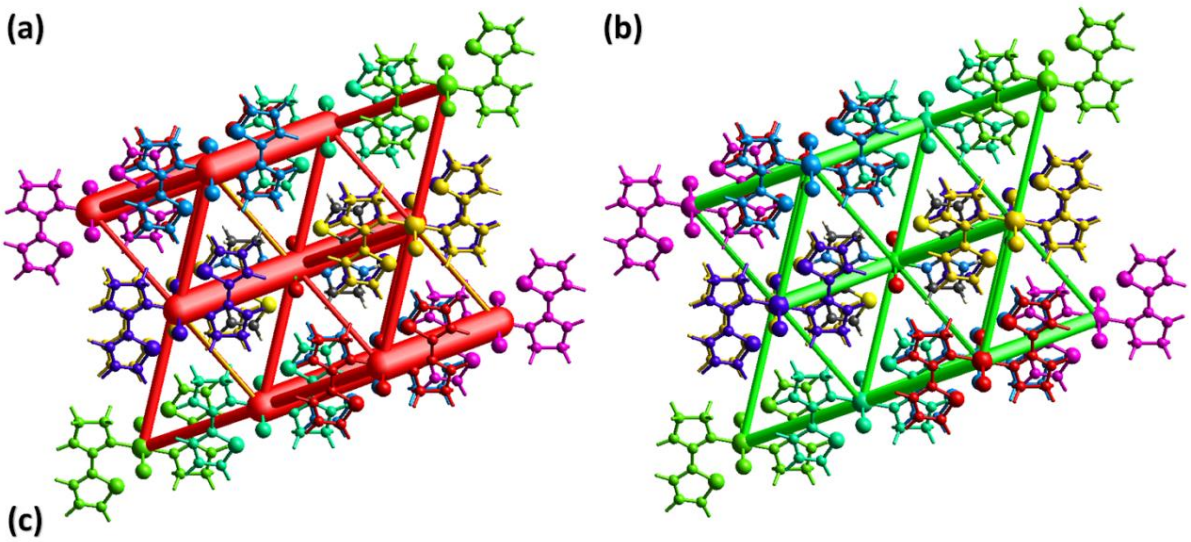

	N	Symop	R	E_ele	E_pol	E_dis	E_rep	E_tot
	2	x, y-1, z+1	8.65	-22.3	-9.0	-8.4	2.0	-34.4
	2	x+1, y-1, z+1	9.23	-46.0	-20.3	-53.8	42.1	-74.4
	2	-x, -y+1, -z+1	15.79	0.0	-0.2	0.0	0.0	-0.2
	2	x+1, y, z	8.77	-41.6	-16.3	-34.9	30.6	-59.6
	2	x, y+1, z-1	8.92	13.9	-2.5	-25.8	6.6	-5.3
	2	x+1, y-1, z	7.98	-118.2	-41.1	-65.9	72.0	-148.2
	2	x, y+1, z+1	12.68	0.0	-1.1	0.0	0.0	-0.7

Fig. 6. Energy frameworks for (a) coulomb electrostatic, (b) dispersion, and (c) interaction energy values with intermolecular distance denoted by R.

Theoretical studies

Geometry optimization

To explore the geometries of species under investigation, their molecular structures were optimized to determine the most stable structure in theoretical calculations using B3LYP/Def2-TZVP. Moreover, in frequency analysis computations, hypothetical frequencies were equal to zero, confirming that the structural optimization of the complex is located at the minimum and lowest local energy points. Figs. 7 and 8 and Table S1 represent the optimized structure of the complex and selected bond lengths and angles in the gas phase, respectively. The evaluation of optimized geometrical features and experimentally calculated parameters show a good agreement.

In the ligand's optimized structure, the lengths of the C=N and C–S bonds are 1.28065 Å and 1.72891

Å, respectively. Their corresponding values in complex structure (gas phase) are 1.28720 Å and 1.72814 Å, which show increasing the length of the C=N bond and decreasing the length of the C–S bond due to complexion.

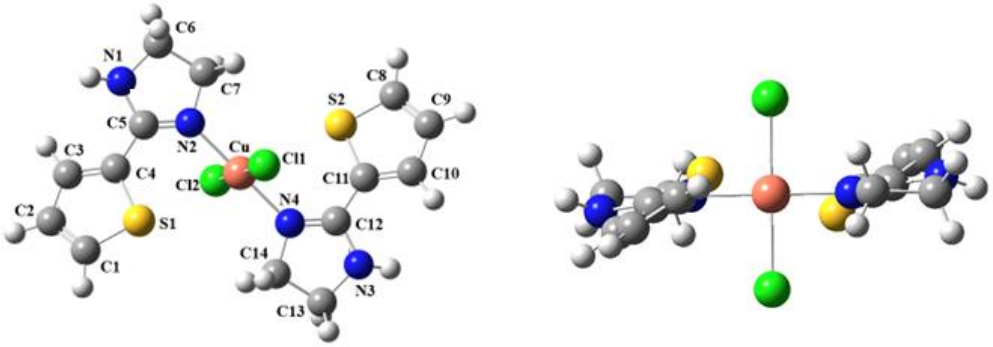

Fig. 7. The upper and sideways visions of the optimized structure of **$CuCl_2(L)_2$** in vacuum using the B3LYP/Def2-TZVP method. The H-atoms linked to the rings are depicted as little white, sulfur atoms in yellow, chlorine atoms in green, nitrogen atoms in blue, and copper atoms in pink spheres.

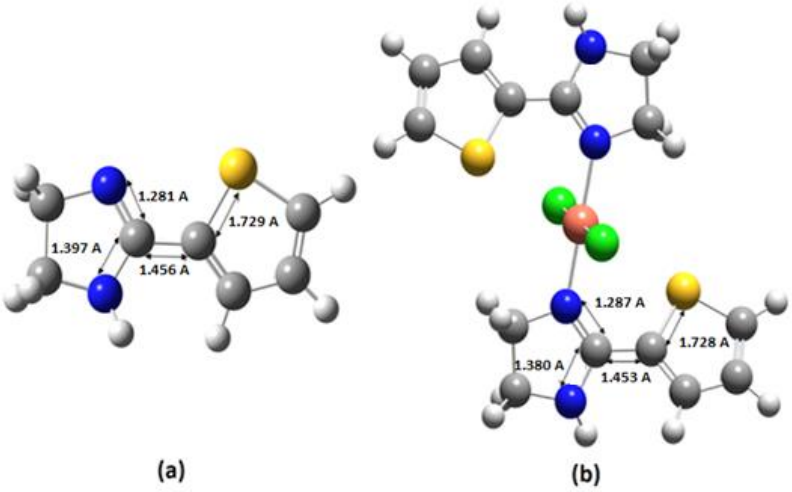

Fig. 8. Bond lengths (a) for the ligand, and (b) for the complex in vacuum.

The analysis of the dihedral angle of the ligand shows that the angle between N=C–C=C is about 8º and almost flat, while this dihedral angle in the gas phase is about 25.12º. As a result, the ligand takes a non-planar structure in the complex structure. Also, the angle between sulfur, copper, and chlorine in the gas phase is smaller than 90º (about 82º).

FT-IR study

Comparing vibrational-stretching frequencies between the complex's calculated values and

experimental data (Fig. S2) reveals notable trends. The N–H stretching frequency increases, the C=C stretching frequency remains relatively constant, and the C–S stretching frequency decreases slightly (Table 5). This comparison exhibits excellent agreement, with a minor difference of approximately 10.73% observed only in the N–H stretching vibration. This discrepancy may arise from doing calculations in the gas phase.

Table 5. The actual and theoretically deliberated infrared vibrational features (cm^{-1}) as well as relative errors of **$CuCl_2(L)_2$** complex.

Assignment	Experimental	Calculated	Relative error (%)[a]
ν N–H	3252	3600	10.70
ν C=N	1597	1645	3.00
ν C=C	1531	1556	1.63
ν C–S	841	861	2.38

[a] Relative error (%) = $(X^{Calc} - X^{Exp}) * 100 / X^{Exp}$.

Frontier molecular orbitals (FMOs)

FMO analysis provides key insights into the kinetic stability and reactivity of molecular species [43]. Notably, the HOMO orbital is distributed on both copper and the ligand, while the LUMO orbital mainly resides on the ligand (Fig. 9), suggesting a potential ligand-to-copper charge transfer. Quantum chemical parameters in Table 6 reveal that **$CuCl_2(L)_2$** exhibits a softer nature with a narrower energy gap (4.19 eV in the gas phase) compared to the ligand (4.76 eV).

This reduced energy gap implies enhanced polarizability, supported by consistent outcomes in chemical hardness and softness. The calculated chemical potential values (-3.86 and -3.70 eV for the ligand and complex, respectively) indicate stability, suggesting resistance to decomposition. Furthermore, the electrophilicity index values highlight the complex's increased electrophilic strength [44,45]. In summary, our concise FMO analysis underscores the ligand-to-copper charge transfer, the softer nature of **$CuCl_2(L)_2$**, and its stability, contributing essential insights into the compound's reactivity.

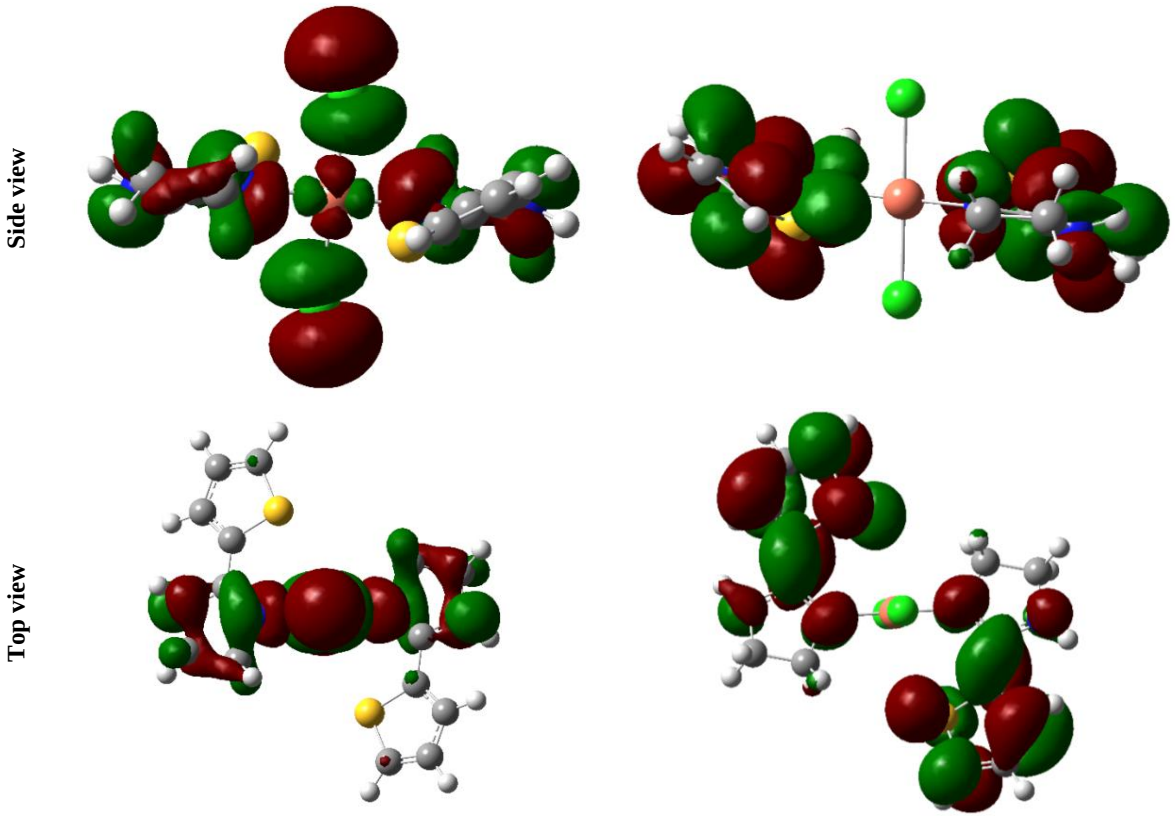

Fig. 9. Frontier molecular orbitals of **$CuCl_2(L)_2$** using the B3LYP/Def2-TZVP method in gas phase.

Table 6. Quantum chemical description of compounds (energies are reported in eV)[a].

Compound	E_{HOMO}	E_{LUMO}	E_{gap}	I	A	η	S	χ	μ	ω
Ligand [22]	-6.24	-1.48	4.76	6.24	1.48	2.38	0.21	3.86	-3.86	3.12
Complex (gas)	-5.80	-1.61	4.19	5.80	1.61	2.09	0.23	3.70	-3.70	3.27

[a] Ionization potential ($I = -E_{HOMO}$); Electron affinity ($A = -E_{LUMO}$); Hardness ($\eta = (I - A)/2$); Softness ($S = 1/2\eta$); Electronegativity ($\chi = (I + A)/2$); Chemical potential ($\mu = -(I + A)/2$); Electrophilicity ($\omega = \mu^2/2\eta$)

Natural bond orbital (NBO) analysis

NBO analysis is a pivotal tool for exploring molecular interactions and charge transfer [46]. Table S2 outlines natural atomic charges, electron configurations and populations (NACs, NECs, and NPs, respectively). The reduction in the initial charge of the Cu ion from +2.0 e to +0.795 e after complexation, indicates a discernible shift of electronic density from nitrogen atomic orbitals to Cu orbitals. This corroborates the charge transfer observed in HOMO and LUMO orbital analyses. Additionally, MEP results highlight positive charge density on the ligand [22], reinforcing the consistent conclusion of charge transfer from the ligand to Cu. Importantly, this NBO analysis enriches our understanding of the electronic structure, emphasizing the dynamic interplay of charge

distribution within the copper complex.

Experimental

Materials and Methods

The various solvents and chemicals used in this investigation are of experimental grade and were acquired from Sigma-Aldrich. The elemental (CHN) study of the ligand and its associated complex with copper was conducted using a Heraeus CHN-O-FLASH EA 1112 device. The stretching vibrational evaluation of synthesized species has been recorded using infrared light by the IRPrestige-21 spectrophotometer. A UP 400S ultrasonic processor with a 3 mm broad and 140 mm long probe that was inserted precisely in a mixture of reacting precursors was utilized for sonication. The ultrasonication took place at 25 ^{o}C in a 40 cm^3 glass reactor.

Synthesis of $CuCl_2(L)_2$ complex

A 15 mL ethanolic solution of the ligand (2 mmol) was added into a 15 mL aqueous $CuCl_2.2H_2O$ solution (1 mmol) and ultrasonicated for 10 min. The resultant green solution was filtered to eliminate undesired solid impurities and left for evaporation under ambient conditions. After one week, green cubic crystals of **$CuCl_2(L)_2$** suitable for diffraction analysis were formed.

$CuCl_2(L)_2$: Yield 87%. Anal. Calc. for $C_{14}H_{16}Cl_2CuN_4S_2$: C, 38.31; H, 3.67; N, 12.77; S, 14.61%, Found: C, 38.46; H, 3.63; N, 12.69; S, 14.72%. FT-IR (KBr, cm^{-1}); 3252 ($\nu_{N–H}$); 1597 ($\nu_{C=N}$); 1531, 1497 ($\nu_{C=C}$); 841 (ν_{C-S}).

Description of X-ray structural solution and refinements of complex

A crystal of proper size was fixed on the Bruker Kappa diffractometer with an APEX II CCD detector. Structural solutions and refinements were achieved on SHELXT-2014 [47] and SHELXL 2019/2 [48], correspondingly. Anisotropic and isotropic displacement factors were given to the atoms denser than hydrogen atoms and hydrogen atoms, respectively. The H-atoms were fixed by applying the

riding model. PLATON [49] is used for structure validation as well as for making ORTEP and packing diagrams. Mercury 4.0 [50] was also employed for graphical purposes. The crystallographic data and the refinement parameters of the complex are shown in Table 1.

Computational details

The Gaussian 09 software has been employed to perform the theoretical computations [51], while the B3LYP functional with a Def2-TZVP basis set was applied for the optimization of the geometry of the copper complex. The same method has previously been chosen to optimize the structure of ligand in the gas phase [22]. Frequency analysis was conducted to validate that the complex structure resides in the most energetically favourable state on the molecular potential energy surface (PES), thereby confirming its stability. The electronic density of state (DOS) of the complex, which represents the electrical characteristics, was acquired using a GaussSum program [52]. The energy gap (E_{gap}) was measured based on the following equation: $E_{gap} = E_{LUMO} - E_{HOMO,}$ where E_{HOMO} and E_{LUMO} are energies of the highest occupied molecular orbital (HOMO) and the lowest unoccupied molecular orbital (LUMO), correspondingly. The contour plots of the HOMO and LUMO were also created by means of the GaussView package [53]. Finally, the obtained molecular electrostatic potential (MEP) outputs were taken into consideration for natural bond orbital (NBO) computations.

Conclusion

2-Thiophenimidazoline ligand is proven to be a significant monodentate ligand to afford the preparation of **$CuCl_2(L)_2$**. The complex shows a sp^2d hybridization to adopt a square planar coordination geometry, which is supported by the respective bond angles around the Cu^{+2} ion acquired from the X-ray data. Based on the dihedral angle, the ligand adopts a non-planar structure upon complexation. The molecules are interconnected *via* N–H···Cl interactions to form dimers, making a loop, which further leads to the formation of infinite C(6) chains. HSA analysis depicts that the most significant contacts are H···H and H···Cl. MEP results highlight positive charge density

on the ligand, reinforcing the consistent conclusion of charge transfer from the ligand to Cu. The FMO analysis was utilized to showcase the chemical reactivity and kinetic stability of the synthesized compound. Additionally, NBO analysis indicates that the charge on the Cu^{+2} decreases from its usual value because of its coordination with the ligand during complexation.

Declarations

Ethical Approval

Not applicable.

Compliance with ethical standards

Conflict of interest: The authors declare that they have no conflict of interest.

Funding

This work received financial support from Ardakan University and Payame Noor University.

Acknowledgments

Ardakan and Payame Noor University provided practical assistance for our project, which we warmly acknowledged.

Appendix A. Supplementary data

CCDC 2268035 holds supplementary crystallographic data for **$CuCl_2(L)_2$**, which can be obtained free of charge through http://www.ccdc.cam.ac.uk/conts/retrieving.html, or from the Cambridge Crystallographic Data Centre, 12 Union Road, Cambridge CB2 1EZ, UK; fax: (+44) 1223-336-033; or e-mail: deposit@ccdc.cam.ac.uk.

References

[1] Mehedi MS, Tepe JJ (2020) Recent advances in the synthesis of imidazolines (2009–2020). Adv Synth Catal 362:4189–4225.

[2] Liu R, Cui J, Ding T, Liu Y, Liang H (2022) Research progress on the biological activities of metal complexes bearing polycyclic aromatic hydrazones. Molecules 27:8393.

[3] Nakamura S, Maeno Y, Ohara M, Yamamura A, Funahashi Y, Shibata N (2012) Enantioselective synthesis of imidazolines with quaternary stereocenters by organocatalytic reaction of N-(heteroarenesulfonyl) imines with isocyanoacetates. Org Lett 14:2960–2963.

[4] Dai L, Zhu Q, Zeng J, Liu Y, Zhong G, Han X, Zeng X (2022) Asymmetric synthesis of chiral imidazolidines by merging copper and visible light-induced photoredox catalysis. Org Chem Front 9:2994–2999.

[5] Szabo B (2002) Imidazoline antihypertensive drugs: a critical review on their mechanism of action. Pharmacol Ther 93:1–35.

[6] Soldatov VO, Shmykova EA, Pershina MA, Ksenofontov AO, Zamitsky YM, Kulikov AL, Peresypkina AA, Dovgan AP, Belousova YV (2018) Imidazoline receptors agonists: possible mechanisms of endothelioprotection. Res Results Pharmacol 4:11–18.

[7] Zhang H, Nie C, Cao D, Cheng X, Guan R (2022) Constructing unconventional fluorescent molecules by imidazoline ring and its salt of carboxylic acid and their application. J Mol Liq 354:118878.

[8] Dardonville C, Rozas I (2004) Imidazoline binding sites and their ligands: an overview of the different chemical structures. Med Res Rev 24:639–661.

[9] Krasavin M (2015) Biologically active compounds based on the privileged 2-imidazoline scaffold: the world beyond adrenergic/imidazoline receptor modulators. Eur J Med Chem 97:525–537.

[10] Romanenko GV, Fursova EY, Letyagin GA, Bogomyakov AS, Petrova MV, Morozov VA, Ovcharenko VI (2018) Crystal structure of metal complexes with 2-imidazoline nitroxides and

dicyanamide. J Struct Chem 59:1412−1420.

[11] Podunavac-Kuzmanović SO, Vojinović LS (2003) Synthesis and physico-chemical characterization of zinc (II), nickel (II) and cobalt (II) complexes with 2-phenyl-2-imidazoline. Acta Period Technol 34:119−124.

[12] Zhao PS, Jian FF, Lu LD, Yang XJ, Wang X, Sundara RS, Fun HK (2000) Synthesis and crystal structure of hexakis(imidazole) cobalt(II) dicinnamate $[Co(C_3H_4N_2)_6](PhCHCHCOO)_2$. Chin J Inorg Chem 16:964−968.

[13] Takroni KM, Farghaly TA, Harras MF, El-Ghamry HA (2020) Synthesis, structure elucidation, DNA binding and molecular docking studies of novel copper (II) complexes of two 1,3,4-thiadiazolethiosemicarbazone derivatives. Appl Organomet Chem 34:e5860.

[14] Osredkar J, Sustar N (2011) Copper and zinc, biological role and significance of copper/zinc imbalance. J Clin Toxicol S3:1−18.

[15] Villarreal W, Colina-Vegas L, Visbal G, Corona O, Correa RS, Ellena J, Cominetti MR, Batista AA, Navarro M (2017) Copper(I)–phosphine polypyridyl complexes: synthesis, characterization, DNA/HSA binding study, and antiproliferative activity. Inorg Chem 56:3781–3793.

[16] Gibson D (2016) Platinum(IV) anticancer prodrugs-hypotheses and facts. Dalton Trans 45:12983–12991.

[17] Avcı D, Altürk S, Sönmez F, Tamer Ö, Basoglu A, Atalay Y, Kurt BZ, Öztürk D, Dege N (2019) A new dinuclear copper (II) complex of 2,5-furandicarboxyclic acid with 4(5)-methylimidazole as a high potential α-glucosidase inhibitor: synthesis, crystal structure, cytotoxicity study, and TD/ DFT calculations. Appl Organomet Chem 33:e4725.

[18] Qin QP, Liu YC, Wang HL, Qin JL, Cheng FJ, Tang SF, Liang H (2015) Synthesis and antitumor mechanisms of a copper (II) complex of anthracene-9-imidazoline hydrazone (9-AIH). Metallomics 7:1124–1136.

[19] Tolman WB (2006) Using synthetic chemistry to understand copper protein active sites: a

personal perspective. J Biol Inorg Chem 11:261–271.

[20] Klema VJ, Wilmot CM (2012) The role of protein crystallography in defining the mechanisms of biogenesis and catalysis in copper amine oxidase. Int J Mol Sci 13:5375–5405.

[21] Kozłowski H, Janicka-Kłos A, Stańczak P, Valensin D, Valensin G, Kulon K (2008) Specificity in the Cu^{2+} interactions with prion protein fragments and related Hisrich peptides from mammals to fishes. Coord Chem Rev 252:1069–1078.

[22] Kargar H, Ashfaq M, Fallah-Mehrjardi M, Behjatmanesh-Ardakani R, Munawar KS, Tahir MN (2022) Synthesis, characterization, SC-XRD, HSA and DFT study of a novel copper(I) iodide complex with 2-(thiophen-2-yl)-4,5-dihydro-1H-imidazole ligand: an experimental and theoretical approach. J Mol Struct 1253:132264.

[23] Hasanova SS, Yolchueva EA, Mashadi AQ, Muhammad S, Ashfaq M, Muhammed ME, Munawar KS, Tahir MN, Al-Sehemi AG, Alarfaji SS (2023) Synthesis, characterization, crystal structures, and supramolecular assembly of copper complexes derived from nitroterephthalic acid along with Hirshfeld surface analysis and quantum chemical studies. ACS Omega 8:8530−8540.

[24] Kargar H, Ashfaq M, Fallah-Mehrjardi M, Behjatmanesh-Ardakani R, Munawar KS, Tahir MN (2022) Theoretical studies, Hirshfeld surface analysis, and crystal structure determination of a newly synthesized benzothiazole copper(II) complex. J Mol Struct 1261:132905.

[25] Kargar H, Ardakani AA, Tahir MN, Ashfaq M, Munawar KS (2021) Synthesis, spectral characterization, crystal structure and antimicrobial activity of nickel(II), copper(II) and zinc(II) complexes containing ONNO donor Schiff base ligands. J Mol Struct 1233:130112.

[26] Kargar H, Aghaei-Meybodi F, Behjatmanesh-Ardakani R, Elahifard MR, Torabi V, Fallah-Mehrjardi M, Tahir MN, Ashfaq M, Munawar KS (2021) Synthesis, crystal structure, theoretical calculation, spectroscopic and antibacterial activity studies of copper(II) complexes bearing bidentate schiff base ligands derived from 4-aminoantipyrine: influence of substitutions on antibacterial activity. J Mol Struct 1230:129908.

[27] Kargar H, Ardakani AA, Munawar KS, Ashfaq M, Tahir MN (2021) Nickel(II), copper(II) and zinc(II) complexes containing symmetrical Tetradentate Schiff base ligand derived from 3,5-diiodosalicylaldehyde: synthesis, characterization, crystal structure and antimicrobial activity. J Iran Chem Soc 18:2493–2503.

[28] Raza H, Yildiz I, Yasmeen F, Munawar KS, Ashfaq M, Abbas M, Ahmad M, Younus HA, Zhang S, Ahmad N (2021) Synthesis of a 2D copper(II)-carboxylate framework having ultrafast adsorption of organic dyes. J Colloid Interface Sci 602:43–54.

[29] Kia R, Fun H-K, Kargar H (2009) 2-(2-Thienyl)-4,5-dihydro-1H-imidazole. Acta Crystallogr Sect E Struct Rep Online 65:o301–o301.

[30] Bernstein J, Davis RE, Shimoni L, Chang NL (1995) Patterns in hydrogen bonding: functionality and graph set analysis in crystals. Angew Chem Int Ed Engl 34:1555–1573.

[31] Spackman PR, Turner MJ, McKinnon JJ, Wolff SK, Grimwood DJ, Jayatilaka D, Spackman MA (2021) CrystalExplorer: a program for Hirshfeld surface analysis, visualization and quantitative analysis of molecular crystals. J Appl Crystallogr 54:1006–1011.

[32] Spackman MA, Jayatilaka D (2009) Hirshfeld surface analysis. CrystEngComm 11:19–32.

[33] Ali A, Din ZU, Ibrahim M, Ashfaq M, Muhammad S, Gull D, Tahir MN, Rodrigues-Filho E, Al-Sehemi AG, Suleman M (2023) Acid catalyzed one-pot approach towards the synthesis of curcuminoid systems: unsymmetrical diarylidene cycloalkanones, exploration of their single crystals, optical and nonlinear optical properties. RSC Adv 13:4476–4494.

[34] Kargar H, Fallah-Mehrjardi M, Behjatmanesh-Ardakani R, Munawar KS, Ashfaq M, Tahir MN (2022) Diverse coordination of isoniazid hydrazone Schiff base ligand towards iron(III): synthesis, characterization, SC-XRD, HSA, QTAIM, MEP, NCI, NBO and DFT study. J Mol Struct 1250:131691.

[35] McKinnon JJ, Jayatilaka D, Spackman MA (2007) Towards quantitative analysis of intermolecular interactions with Hirshfeld surfaces. Chem Commun 3814–3816.

[36] Haroon M, Baig MW, Akhtar T, Tahir MN, Ashfaq M (2023) Relativistic two-component time

dependent density functional studies and Hirshfeld surface analysis of halogenated arylidenehydrazinylthiazole derivatives. J Mol Struct 1287:135692.

[37] Al-Jibori SA, Al-Jibori GHH, Ashfaq M, Khalil T, Laguna M, Wagner C, Tahir MN, Al-Janabi ASM (2023) Synthesis, characterization, crystal Structure, Hirshfeld surface analysis of Cd(II)-1,2-benzisothiazol-3(2H)-one complexes. J Mol Struct 135803.

[38] Jelsch C, Ejsmont K, Huder L (2014) The enrichment ratio of atomic contacts in crystals, an indicator derived from the Hirshfeld surface analysis. IUCrJ 1:119–128.

[39] Kargar H, Ashfaq M, Fallah-Mehrjardi M, Behjatmanesh-Ardakani R, Munawar KS, Tahir MN (2022) Unsymmetrical Ni(II) Schiff base complex: synthesis, spectral characterization, crystal structure analysis, Hirshfeld surface investigation, theoretical studies, and antibacterial activity. J Mol Struct 1265:133381.

[40] Mackenzie CF, Spackman PR, Jayatilaka D, Spackman MA (2017) CrystalExplorer model energies and energy frameworks: extension to metal coordination compounds, organic salts, solvates and open-shell systems. IUCrJ 4:575–587.

[41] Turner MJ, Grabowsky S, Jayatilaka D, Spackman MA (2014) Accurate and efficient model energies for exploring intermolecular interactions in molecular crystals. J Phys Chem Lett 5:4249–4255.

[42] Tahir MN, Ashfaq M, Ali A, Lai CH, Rao BR, Shahid IA, Munawar KS (2023) Synthesis, SC XRD based structure elucidation, supramolecular assembly exploration via Hirshfeld surface analysis, computational and QTAIM study of functionalized anilide. Acta Chim Slov 70:281–293.

[43] Tabares-Mendoza C, Guadarrama P (2006) Predicting the catalytic efficiency by quantum-chemical descriptors: theoretical study of pincer metallic complexes involved in the catalytic Heck reaction. J Organomet Chem 691:2978–2986.

[44] Geerlings P, De Proft F, Langenaeker W (2003) Conceptual density functional theory. Chem Rev 103:1793–1874.

[45] Tzouras NV, Neofotistos SP, Vougioukalakis GC (2019) Zn-Catalyzed multicomponent KA2 coupling: one-pot assembly of propargylamines bearing tetrasubstituted carbon centers. ACS Omega 4:10279–10292.

[46] Wei L, She Y, Yu Y, Yao X, Zhang S (2012) Substituent effects on geometric and electronic properties of iron tetraphenylporphyrin: a DFT investigation. J Mol Model 18:2483–2491.

[47] Sheldrick GM (2015) SHELXT–Integrated space-group and crystal-structure determination. Acta Crystallogr Sect A Found Adv 71:3–8.

[48] Sheldrick GM (2015) Crystal structure refinement with SHELXL. Acta Crystallogr C Struct Chem 71:3–8.

[49] Spek AL (2009) Structure validation in chemical crystallography. Acta Crystallogr D Biol Crystallogr 65:148–155.

[50] Macrae CF, Sovago I, Cottrell SJ, Galek PT, McCabe P, Pidcock E, Platings M, Shields GP, Stevens JS, Towler M (2020) Mercury 4.0: from visualization to analysis, design and prediction. J Appl Crystallogr 53:226–235.

[51] Frisch MJ, Trucks GW, Schlegel HB, Scuseria GE, Robb MA, Cheeseman JR, Scalmani G, Barone V, et al. (2016) Gaussian 09, Revision A.02, Gaussian, Inc., Wallingford CT.

[52] http://www.chemissian.com

[53] Dennington R, Keith TA, Millam JM (2016) GaussView, Version 6, Semichem Inc., Shawnee Mission, KS.